Ion/electron redistributed 3D flexible host for achieving highly reversible Li metal batteries

Huai Jiang, Yangen Zhou, Caohong Guan, Maohui Bai, Furong Qin, Maoyi Yi, Jie Li, Bo Hong, Yanqing Lai**

H. Jiang, Y. Zhou, M. Bai, F. Qin, M. Yi, J. Li, B. Hong, Y. Lai

School of Metallurgy and Environment

Central South University

Changsha 410083, Hunan, China

E-mail: bop_hong@csu.edu.cn, laiyanqing@csu.edu.cn

C. Guan

University of Michigan–Shanghai Jiao Tong University Joint Institute

Shanghai Jiao Tong University

800 Dongchuan Road, Shanghai 200240, China

B. Hong, Y. Lai

Engineering Research Centre of Advanced Battery Materials

The Ministry of Education

Changsha 410083, Hunan, China

Keywords: Li metal anode, CoP, Metal-organic frameworks, ion/electron redistribution, high reversibility

ABSTRACT: Three-dimensional (3D) carbon frameworks are promising hosts to achieve highly reversible lithium (Li) metal anodes, whereas insufficient effects are attributed to their single electron conductivity caused local aggregating of electron/Li^+ and uncontrollable Li dendrites. Herein, an ion/electron redistributed 3D flexible host is designed by lithiophilic carbon fiber cloth modified with MOF-derived porous carbon sheath with embedded CoP nanoparticles (CoP-C@CFC). Theory calculations demonstrate the strong binding energy and plenty of charge transfer from the reaction between CoP and Li atom are presented, which is beneficial to in-situ construct Li_3P@Co ion/electron conductive interface on every single CoP-C@CFC. Thanks to the high ionic conductive Li_3P and electron-conductive Co nanoparticles, the rapid dispersion of Li^+ and obviously reduced local current density could be achieved simultaneously. Furthermore, in-situ optical microscopy observations display obvious depression for volume expansion and Li dendrites. As expected, a miraculous average Coulombic efficiency (CE) of 99.96% over 1100 cycles at 3 mA cm^{-2} and a low overpotential of 11.5 mV with prolonged cycling of over 3200 h at 20% depth of discharge (DOD) are successfully obtained. Consequently, the CoP-C@CFC-Li||$LiFePO_4$ full cells maintain a capacity retention of 95.8% with high CE of 99.96% over 500 cycles at 2C and excellent rate capability.

1. Introduction

The ambitious goal of being carbon neutral all over the world will strongly drive the electrification of the automobile, so that more efficient energy storage systems are urgently needed.[1,2] Compare to current Li-ion batteries consisted of graphite anode (350–400 W h kg^{-1}), Li

metal batteries matched with Li metal anodes exhibit an irresistible attraction due to high energy densities (3500 W h kg^{-1} in Li-air battery, and 2600 W h kg^{-1} in Li-S battery).[3,4] However, poor cycling reversibility and potential safety hazards from Li dendrite growth limit its practical application, which are ascribed primarily to non-uniform Li deposition and huge volume effect.[5] To overstride these obstructions, considerable efforts have been devoted, including tailoring new electrolytes and additives to in-situ form robust SEI layers[6,7], constructing solid state electrolytes to hinder Li dendrites,[8,9] regulating appropriate external factors (temperature,[10] pressure[11] or current density[12]), designing novel 3D Li metal[13,14] and ingenious porous metal current collectors.[15,16] Although Li dendrites could be partially suppressed via these strategies, highly reversible Li plating/stripping is still difficult to realize effectively under realistic current density with high capacity.

Fortunately, the 3D carbon frameworks with large specific area not only decrease local current density and hinder Li dendrite growth, but also depress huge volume expansion, contributing to achieve highly reversible Li metal anodes with high energy density.[17] Thus, all kinds of novel 3D carbon matrixes, such as carbon fibers,[18,19] 3D graphene-based skeletons[20] and hollow carbon sphere,[21] have been verified. Among them, benefitting from the excellent mechanical property, free-standing, low-cost and easy to large-scale production, carbon fiber cloth displays an enormous practical potential to as a high-performance host of Li metal anode.[22,23] However, as-fabricated 3D carbon frameworks are mostly single electron-conductive skeletons, which induces inhomogeneous electron accumulation and then drives Li^+ non-unform distribution or transfer on the surface of carbon fiber cloth as shown in Fig. 1a. It leads to dendritic Li accumulating on the surface of electrode and most of the 3D void being not fully utilized.[24-26] Despite lithiophilicity modification with precious or transition metal (Au,[27] Ni,[28] Ag[29]), transition metal oxides (ZnO,[30] RuO_2,[31] NiO[32]), metal sulfides (Cu_7S_4),[33] metallic nitrides (Ni_xN[34]) inducing Li selective deposition could partially settle these problems, this phenomenon of ion/electron maldistribution is hard to change in essence. Besides, lithiophilic materials with these disadvantages of high cost and easy to structural failure hider its commercial application. Recently, MOF derivates with weak conductivity acting as inert sheath in-situ enfold the carbon fiber cloth core to low local current density and change uneven charge distribution of electrode interface.[35,36] Furthermore, abundant lithiophlic sites as

nucleation seeds guide Li uniform deposition.[37,38] However, owing to the single electron-conductive carbon skeleton and the as-formed insulated Li_2O caused large polarization, which usually is harmful for uniform Li plating/stripping.[39,40] To fundamentally settle the problem of ion/electron uneven distribution on 3D carbon fibers, there is still an urgent demand to explore a high-efficiency carbon fiber host with superior structural stability, lithiophilicity and 3D mixed ion/electron conductivity.

Here, we construct a MOF-derived porous carbon sheath with embedded CoP nanoparticles modified carbon fiber cloth (CoP-C@CFC) (Fig. 1b), whose electrode interface is further transferred to Co particles surrounded by Li_3P networks through the lithiation of CoP nanoparticles, in-situ forming a 3D mixed ion/electron conductive interface (MICI) for interfacial charge and Li^+ redistribution. Importantly, the CoP-C@CFC shows multiple findings: (1) weakly conductive MOF-derived porous carbon sheath is regarded as insulated 'outerwear', which weakens space charge polarization of pure carbon fiber cloth (CFC) (Fig. 1a) and uniforms Li^+/electron flux into entire 3D skeletons. (2) Density functional theory (DFT) calculations demonstrate that stronger binding energy from the reaction between CoP and Li atom (-6.4 eV) and a plenty of charge transfer as shown in Fig. 1c-d, thus driving the forming of Li_3P@Co ion/electron conductive interface. (3) the fast ionic conductive Li_3P (10^{-4} S cm^{-1}) and electron-conductive Co nanoparticles to homogenize the Li^+ flux and charge distribution on the surface of CoP-C@CFC during the repeated Li plating/stripping (Fig. 1b). (4) the lithiophilic CoP and reversible Li_3P product effectively eliminate nucleation barriers and form robust SEI layer, which are helpful to achieve permanent Li affinity and smooth Li layer with high reversibility. (5) a strong and flexible carbon scaffold to suffer huge pressure fluctuations and depress volume effect. Therefore, the well-designed carbon fiber skeletons achieve an amazing high average CE of 99.96% with a sustainable lifespan of 1100 cycles at practical current density of 3 mA cm^{-2}. Moreover, the symmetric batteries with limited CoP-C@CFC-Li composite anodes also present a very low overpotential of 11.5 mV over 3200 h at 1 mA cm^{-2} with 1 mAh cm^{-2} (20% DOD). Coupled with $LiFePO_4$ (LFP) cathode, the CoP-C@CFC-Li||LFP full cells hold a capacity retention of 95.8% with 130 mAh g^{-1} over 500 cycles at 2C and excellent rate capability. Based on these advantages, CoP-C@CFC is an extremely promising candidate for high specific capacity, large-scale, and high-performance Li metal anodes.

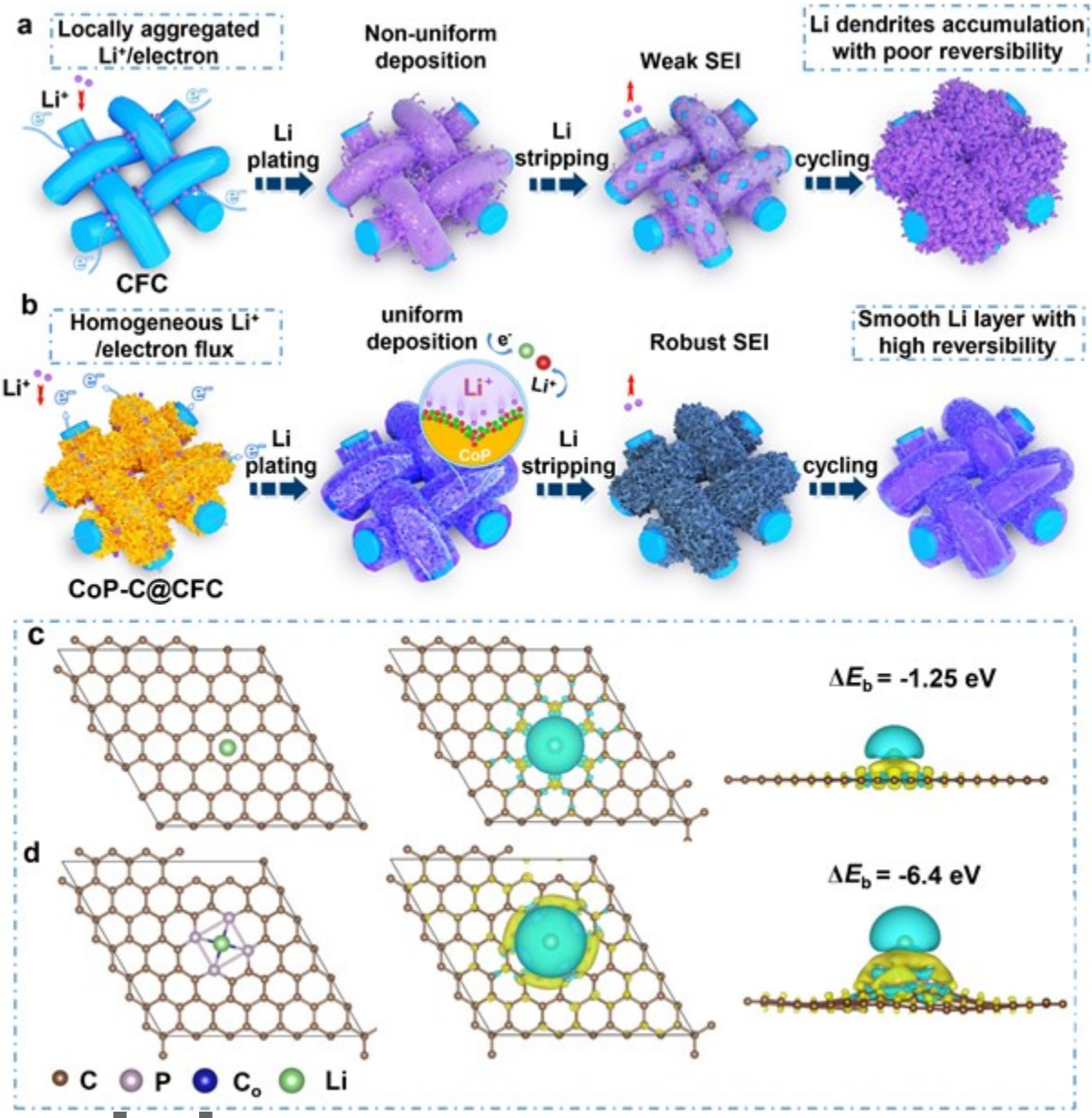

Fig. 1. Li plating/stripping process on pure CFC (a) and CoP-C@CFC (b) electrode; Binding energies of a Li atom with CFC (c) and CoP-C@CFC (d) at the top sites by density functional theory calculations.

2. Results and Discussion

As Fig. 2a shown, CoP-C@CFC was fabricated by a scalable room-temperature crystallization and annealing-phosphating process.[41,42] In brief, Co-MOF (ZIF-67) nanoflakes arrays were in-situ

grown onto the CFC via a facile solution crystallization method using mixing a given amount of $Co(NO_3)_2 \cdot 6H_2O$ and 2-methylimidazole (2-MeIm) in aqueous solution at room temperature. 2D Co-MOF nanoflakes arrays uniformly covered on the smooth surface of pure carbon fiber cloth wiped off by acid solution (Fig. 2b). As depicted in Fig. 2c, plenty of the regular Co-MOF nanoflakes arrays grow vertically on the CFC (Co-MOF@CFC), which is just like beautiful hydrangea. Subsequently, the Co-MOF precursor was annealed in Ar and Air atmosphere successively, during which the organic ligands were chemically transformed into porous carbon sheath and Co_3O_4 nanoparticles (Fig. S1) were evenly anchored (Co_3O_4-C@CFC). Then, the Co_3O_4-C@CFC is further transformed into CoP-C@CFC through low

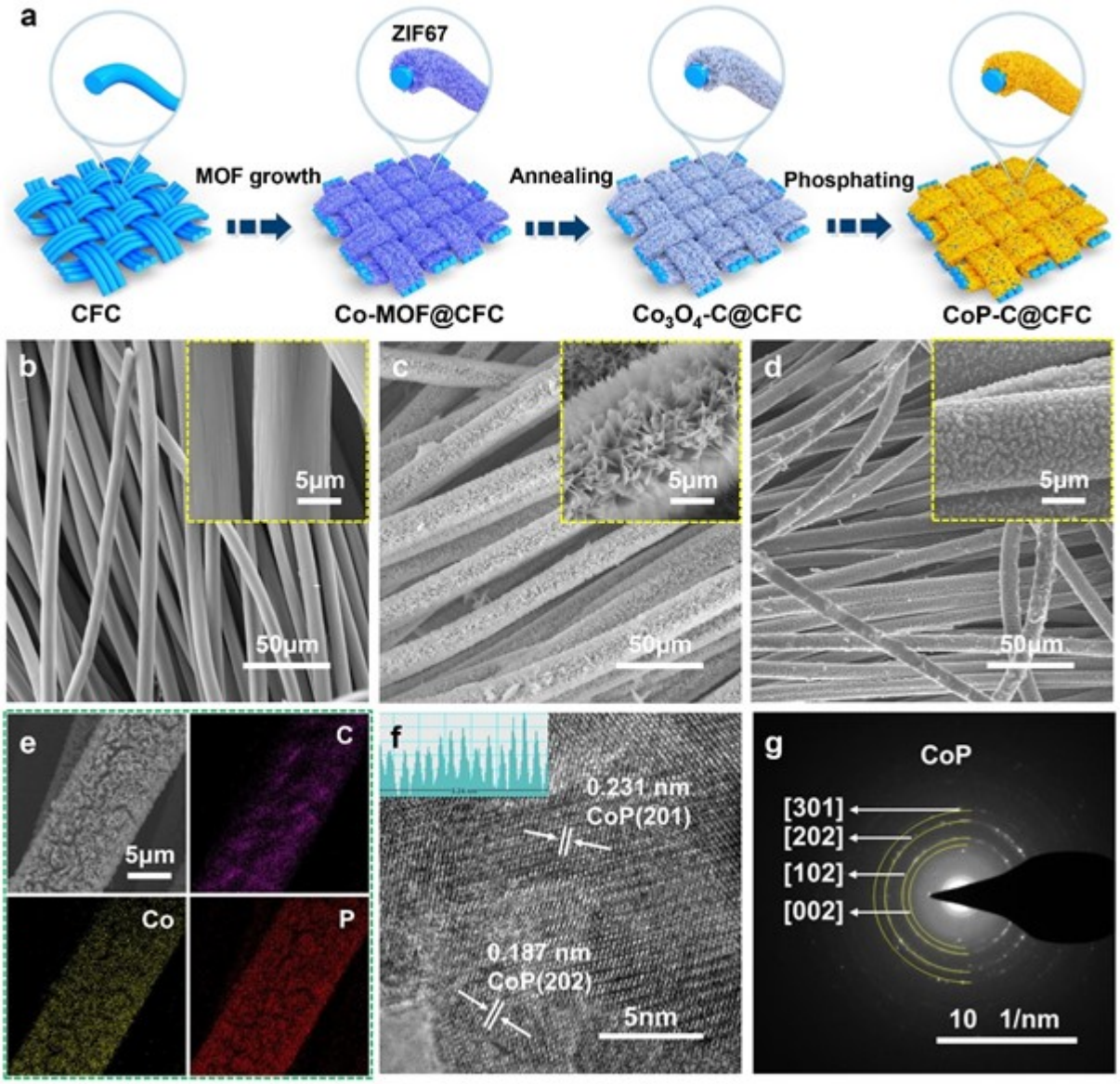

Fig. 2. (a) Schematic of the preparation process of CoP-C@CFC. SEM images of b) CFC, c) Co-MOF@CFC, and d) CoP-C@CFC. (e) Elemental mapping of C, P, and Co elements in a single CoP-C@CFC. HRTEM (f) and SAED (g) of the CoP-C@CFC.

temperature phosphating under Ar atmosphere. Eventually, smooth carbon fibers skeletons were uniformly covered by interlaced CoP nanoflakes with abundant microporosity (Fig. 2d), whose thickness is about 4.8 μm (Fig. S2) indicating compact and steady 3D composite carbon frameworks. Phase changes are also reflected in the color of the carbon fiber cloth. The gray pure CFC turns to

purple and black successively (Fig. S3), which owes to the composited Co-MOF precursor and porous carbon sheath with embedded CoP nanoparticles (CoP-C), respectively. Additionally, inappropriate solution concentration and soaking time affect the in-situ growth of Co-MOF nanoflakes on the CFC (Fig. S4), which subsequently forms undesired CoP embedded carbon nanosheets (Fig. S5) and falls to fabricate CoP sheath. From EDX spectrograms (Fig. S7) and element mapping images (Fig. 2e), the matched spatial distributions of C, P and Co elements are exhibited, which further confirms the uniform coating of CoP-C on CFC skeleton. CoP nanoparticles with a particle size of about 15 nm could be found uniformly embedded in the carbon nanosheets (Fig. S6). High-resolution TEM (HRTEM) characterization reveals unambiguous lattice fringe with the spacing of 0.187 nm, corresponding to the (111) plane of CoP (Fig. 2f). Furthermore, the legible diffraction ring is showed in the selected-area electron diffraction (SEAD) pattern, which further testifies the high crystallinity of CoP (Fig. 2g).

The phase structures of CFC, Co-MOF@CFC and CoP-C@CFC are further confirmed by the X-ray diffraction (XRD) patterns in Fig. 3a. There are two clear broad peaks at about 24.5° and 43.8° shown in XRD result of CFC, which indicates poor crystallization. Co-MOF in-situ grows onto the CFC, whose phase is tested by the comparison of the XRD results between Co-MOF@CFC and simulated Co-MOF. After annealing-phosphating process, CoP-C@CFC is successfully achieved with obvious characteristic peaks of CoP. CoP-C@CFC also presents high specific surface area of 60.517 m^2/g from the results of Brunauer-EmmettTeller (BET) test (Fig. 3b), which is 23 times as much as CFC. It indicates MOF-derived porous carbon sheath with embedded CoP nanoparticles effectively enhance specific surface area of carbon fiber skeletons, which is beneficial to higher Li capacity and lower local current density. In addition, the pore size distribution displays plenty of micropores/mesopores of ~20 nm originated from porous carbon sheath with embedded CoP nanoparticles, which provides abundant Li nucleation interface and loading space of Li metal (Fig. S8). The surface chemical composition and status of CoP-C@CFC are further investigated by X-ray photoelectron spectroscopy (XPS). As shown in Fig. S9, the characteristic peaks of C, O, Co, and P are clearly presented, indicating these elements co-existence. In Fig. 3c, two clear characteristic peaks located at 778.0 and 781.1 eV are indexed to Co $2p_{3/2}$. Another strong peak located at 796.9 eV is corresponding to

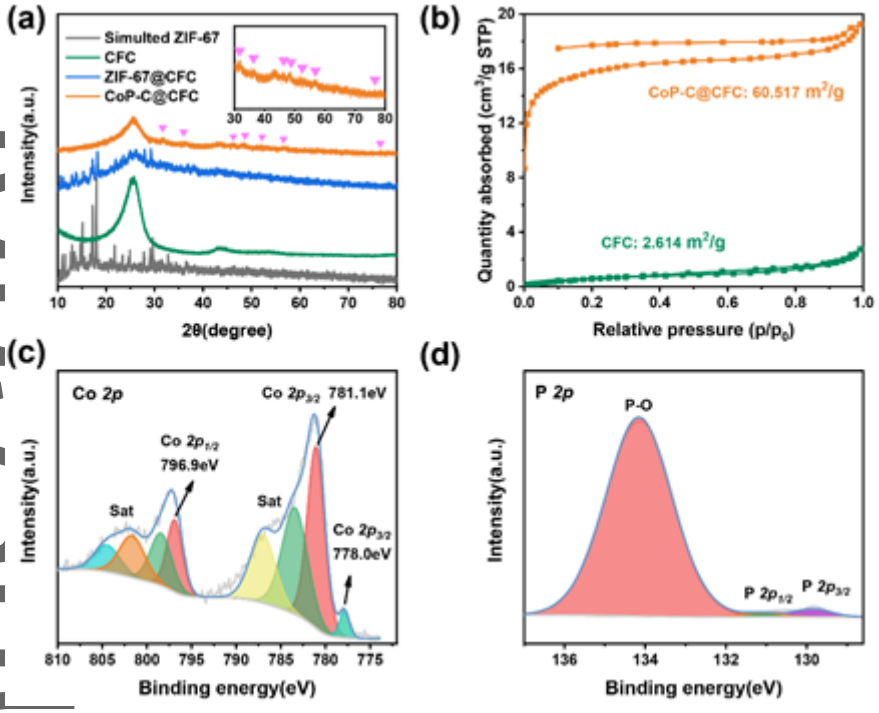

Fig. 3. Characterization of CoP-C@CFC. (a) XRD patterns of CFC, Co-MOF@CFC and CoP-C@CFC. (b) N_2 adsorption–desorption isotherm curve of CoP-C@CFC. XPS spectra of the CoP-C@CFC of (c) Co 2p and (d) P 2p.

Co $2p_{1/2}$. The peaks at 778.0 and 796.9 eV are close to the binding energies of Co into CoP.[43]

Additionally, owing to the shake-up excitation of the high-spin Co^{2+}, the satellite peaks are observed at 783.4, 787.0, 798.4, 801.7, 804.2 eV. In Fig. 3d, the characteristic peaks of P $2p_{1/2}$ and P $2p_{3/2}$ situated at 131.1 and 129.7 eV, which is relate to Co-P.[44] The clear species of the P-O compound is confirmed by the strong peak of 134.1 eV, which is attributed to oxidation.

To preliminarily testify the lithiophilicity of CoP-C@CFC, binding energy (E_b) of a Li atom with CoP in CoP-C@CFC or pure carbon fiber cloth (CFC) is estimated by density functional theory (DFT) calculations. As Fig. 1c shown, Li atom adsorbs on the optimal structure of pure carbon, which displays the calculated binding energy (ΔE_b) of -1.25 eV. Comparatively, the calculated binding energy of Li atom (T sites) with the optimal structure of CoP is -6.4 eV (Fig. 1d), which is higher than ΔE_b of Li atom at H sites (Fig. S10) indicating superior Li affinity relative to pure carbon. Compared to

CoP-C@CFC, Co_3O_4-C@CFC presents the lower ΔE_b of -4.62 eV and higher nucleation overpotential of 9 mV (Fig. S11), which elucidates the better lithiophilicity of CoP-C@CFC. In addition, the electron accumulation and depletion between Li with pure CFC or CoP-C@CFC also are shown in Fig. 1c-d. In the 3D mode of Li atom adsorption, the yellow and light blue regions represent electron reduction and accumulation, respectively. Compared with pure carbon, amount of charge spontaneously transfers from Li atom to CoP-C@CFC substrate, which reveals stronger bond capability between Li and CoP-

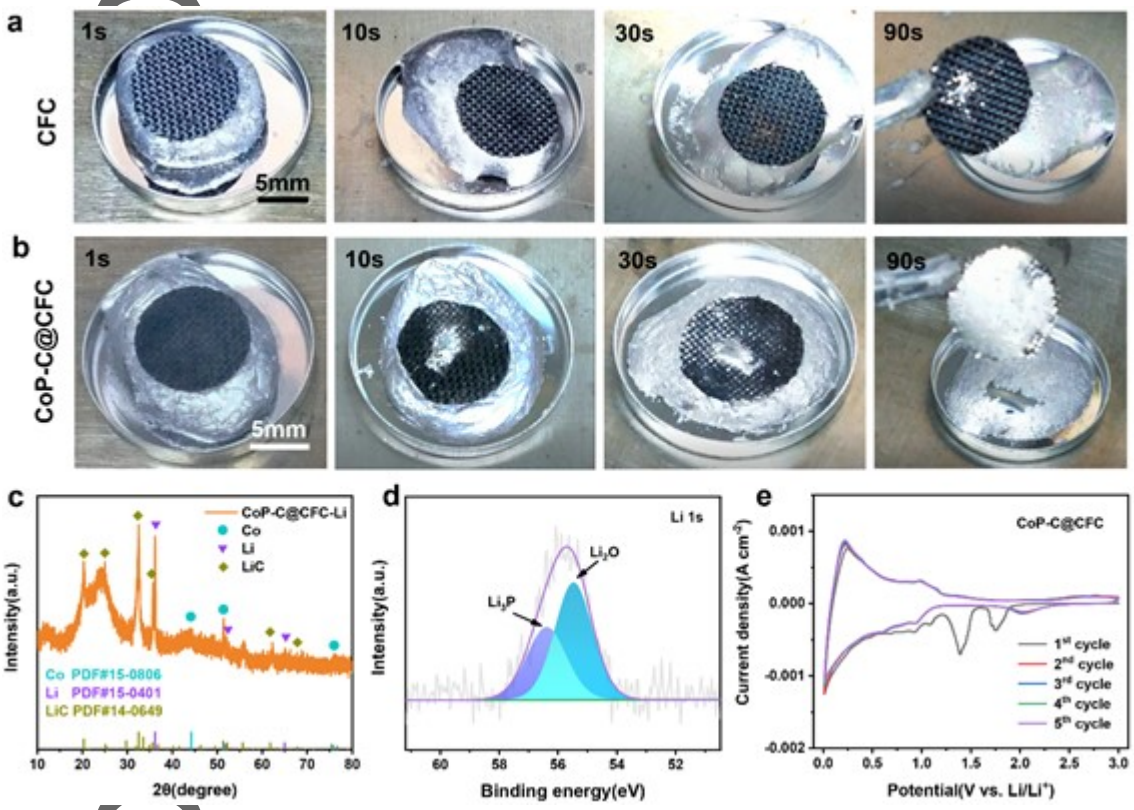

Fig. 4. The lithiophilicity test of CoP-C@CFC. Wettability comparison of molten Li onto CFC (a) and CoP-C@CFC (b) substrates. (c) the reaction product of CoP-C@CFC and Li metal. (d) high-resolution XPS spectra of Li 1s to study the interfacial composition of CoP-C@CFC-Li. (e) The cyclic voltammogram of CoP-C@CFC during the initial five cycles from 3.0 to 0.01V.

C@CFC. To intuitively verify lithiophilicity of CoP-C@CFC host, the wettability test of molten Li infusing CFC and CoP-C@CFC are performed. As shown in Fig. 4a, the CFC substrate have not been

wetted obviously in 90 seconds and displays poor blend faculty, owing to the 'lithiophobic' nature of pure carbon. By contrast, CoP-C@CFC host contacts the molten Li to exhibit prominent Li affinity, whose disk center is rapidly infused liquid Li (Fig. 4b). After 10 seconds, the molten Li has permeated carbon fibers layer presenting silvery character. Liquid Li metal continues to along with every single carbon fiber to diffuse in 30 seconds (Fig. S12a), which displays contact angle of zero between Li metal and CoP-C@CFC substrate. Finally, Li metal uniformly spreads out entire surface of CoP-C@CFC electrode (Fig. S12b) and has successfully blended with each other after 90 seconds, while little Li metal attach on the surface of CFC. Therefore, the above theoretic calculations and wettability results demonstrate CoP-C@CFC has outstanding lithiophilicity, which will benefit homogeneous Li nucleation and deposition along the surface of the carbon fibers due to the more favorable energy. To further study the nature of lithiophilicity, electrodeposition is performed to fabricate the 3D composite Li metal anode of CoP-C@CFC-Li, whose component is further characterized with XRD and XPS. The peaks of well-crystallized Co phase are clearly found in XRD pattern, while the peak of Li_3P is not obviously detected due to the low crystallization (Fig. 4c). To deeply verify the formation of Li_3P phase, high-resolution XPS spectra of Li 1s is introduced in Fig. 4d. Obviously, the peaks located at 56.9 eV are assigned to the generation of Li-P bonds,[25,45] and Li_3P phase turns to be the dominant components for fast Li^+ distribution (Fig. 4d).[46] Correspondingly, the cyclic voltammetry (CV) curves of CoP-C@CFC within the potential ranging from 3.0 to 0.01V in initial five cycles are presented in Fig. 4e. In the first cathodic scan, the peak at 1.75 V is attributed to the lithiation of carbon-oxygen functional groups.[47] When the voltage drops at 1.4 V, the appearance of a broad irreversible reduction peak could owe to a transition phase of Li_xCoP formed by the lithium intercalation of the CoP.[48] With the scan voltage below 1 V, the successive slope can be related to the continuous transformation to Co and Li_3P accompanying with some irreversible reactions related with the solid electrolyte interphase (SEI) film.[49] In the first cycle of the oxidation process, the Li_3P is delithiated corresponding to the peak located at 1.1 V. After the first cycle, due to the structural reconstruction of the active material, the broad cathodic peak in the range 1.75−0.5 V shifts to 2.0 and 0.6 V during the following cycles, which corresponds to the formation of Li_xCoP and Li_3P. This is a common phenomenon for the conversion-type anode materials. The anodic peak at 1.1 V is assignable to the reversible reaction to CoP.[43] The following CV curves are stable and reproducible, indicating a good reversibility of CoP-C@CFC. Thus, the reaction mechanism has be revealed: (1) CoP

+ $xLi^+ + xe^- \leftrightarrow Li_xCoP$; (2) $Li_xCoP + (3-x)\ Li^+ + (3-x)\ e^- \leftrightarrow Li_3P + Co$. Benefitting from constructed ion/electron conductive interface of Li_3P@Co on the CoP-C@CFC electrode,[24,25,50] outstanding Li affinity and Li^+ diffusion kinetics could be achieved simultaneously. Moreover, CoP-C@CFC electrode displays the nucleation overpotential of 7.4 mV (Fig. S13), which is obvious lower than CFC electrode (23.3 mV).

To further understand the effect of CoP-C@CFC on Li deposition behavior, the morphology evolutions of Li plating on Li foil, CFC and CoP-C@CFC electrode were studied by in-situ and ex-situ technologies. As depicted in Fig. 5b, Li prefers to uneven nucleation and deposition on the interface of separator/CFC electrode due to inhomogeneous pristine carbon fibers (Fig. 5a), causing much dendritic Li to form. When the Li deposition capacity is raised to 5 mAh cm^{-2}, mosslike Li dendrites overspread the entire CFC electrode (Fig. 5c). With the capacity further increasing to 10 mAh cm^{-2}, a mass of Li dendrites accumulates on the surface of CFC leading to the plugging of pore space (Fig. 5d). Comparatively, Li uniformly plates on every single carbon fiber modified with MOF-derived porous carbon sheath with embedded CoP nanoparticles (Fig. 5e), which displays dendrite-free Li deposition in Fig. 5f. When the Li

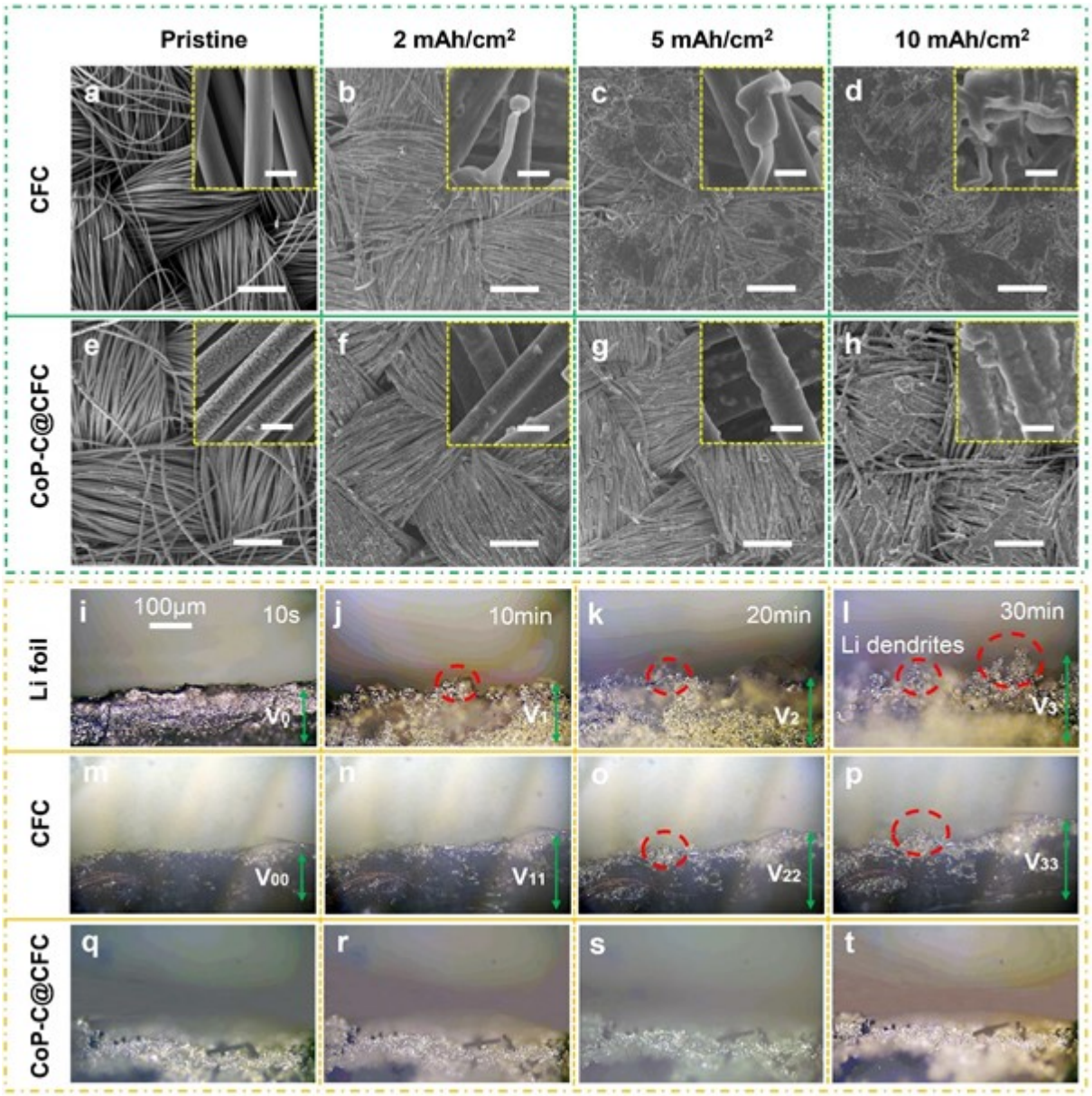

Fig. 5. The morphologies of CFC and CoP-C@CFC electrode by plating Li metal with different capacity at 0.5 mA cm^{-2}. SEM images of CFC (a-d) and CoP-C@CFC (e-h) electrode with 0, 2, 5 and 10 mAh cm^{-2}, respectively. In situ optical microscopy observations of the Li deposition process with Li foil (i-l), CFC-Li (m-p) and CoP-C@CFC-Li (q-t) as electrodes at 3 mA cm^{-2}. The scale bars are 10 μm in yellow dotted box, the others are 200 μm.

metal of 5 mAh cm^{-2} is deposited, the diameter of every single CoP-C@CFC becomes significantly larger due to covered evenly Li metal layer. Despite the capacity of 10 mAh cm^{-2} is further executed, Li metal still uniformly spreads over whole 3D carbon frameworks without dendritic Li accumulating. From the cross-section of the electrode, the diameter of every single CoP-C@CFC obviously increases in varying degrees after deposited with the capacity of 2 or 5 mAh cm^{-2} compared with pristine (Fig. S14a-c). When the deposition capacity is raised to 10 mAh cm^{-2} (Fig. S14d), homogeneous Li metal fills with the gap of carbon fiber cloth without Li dendrites (Fig. S15). Furthermore, the thickness of the electrode is not obvious change (Fig. S14e-h). It indicates CoP-C@CFC host possesses markedly superior Li affinity and the regulating capability of Li deposition. To deeply explore Li growth behavior and volume effect on CoP-C@CFC electrode, in situ optical microscopy is used to record the dynamic process of Li deposition. Initially, the capacity of 10 mAh cm^{-2} is pre-deposited in CFC and CoP-C@CFC, which is used to assembled symmetric cells. For pure Li foil, we can see a relative flat surface and compact structure at 10 seconds (Fig. 5i). However, as Li foil is plated from 10 to 30 minutes (Fig. 5j-l), the surface of Li foil electrode becomes fleeciness accompanying with obvious Li dendrites in the red dotted circle. The thickness of Li foil is raised to 1.5 times relative to pristine after continuous plating of 30 minutes, which presents simultaneously huge volume effect. Similarly, conspicuous Li dendrites and volume change also occur in CFC-Li electrode, whose thickness is increased to near 2 times (Fig. 5m-p). Compared with pure Li foil, Li dendrites on CFC electrode begin to form 10 minutes late (Fig. 5o), which means CFC can delay the forming of Li dendrites due to large specific area and lower local current density. Distinctively, CoP-C@CFC-Li electrode exhibits ultra-stable Li plating accompanying with dendrite-free alongside with almost no volume expansion throughout the whole process (Fig. 5q-t). It indicates MOF-derived porous carbon sheath with embedded CoP nanoparticles guides uniform Li deposition, inhibiting Li dendrites and volume effect.

The electrochemical performance of CoP-C@CFC is evaluated by half-cell and symmetric-cell. As shown in Fig. 6a, the CFC electrode displays a low average CE of 96.3% with rapidly terminative cycling lifespan at 3 mA cm^{-2} with the capacity of 1 mAh cm^{-2}, which possibly is caused by inhomogeneous Li deposition induced plenty of 'dead' Li. When the capacity of Li deposition is raised to 2 mAh cm^{-2}, the CFC electrode can maintain relative stability, whereas the CE appears drop

dramatically in 100 cycles due to Li dendrites accumulation leading to short circuit. Similarly, unstable CE and short cycling life are further deteriorated at 5 mA cm^{-2} with the capacity of 3 mAh cm^{-2}, which reveals poor electrochemical performance. By contrast, the CoP-C@CFC electrode shows an ultra-stable average CE of 99.96% with ultralong cycle life of over 1100 cycles. Although the capacity of Li plating/stripping increases to 2 mAh cm^{-2}, a high average CE of 99.67% still can maintains. Even at higher current density of 5 mA cm^{-2} with the practical cycling capacity of 3 mAh cm^{-2}, CoP-C@CFC electrode keeps superior average CE of 99.42% over 250 cycles. In Voltage-capacity profiles, CoP-C@CFC electrodes (Fig. S16) also exhibit obviously lower polarization voltage and more stable capacity retention than CFC electrodes (Fig. S17). Although the test temperature is increased to 60℃, the CoP-C@CFC electrode can keep 425 cycles with a high average CE 99.2% at 5 mA cm^{-2} with a total

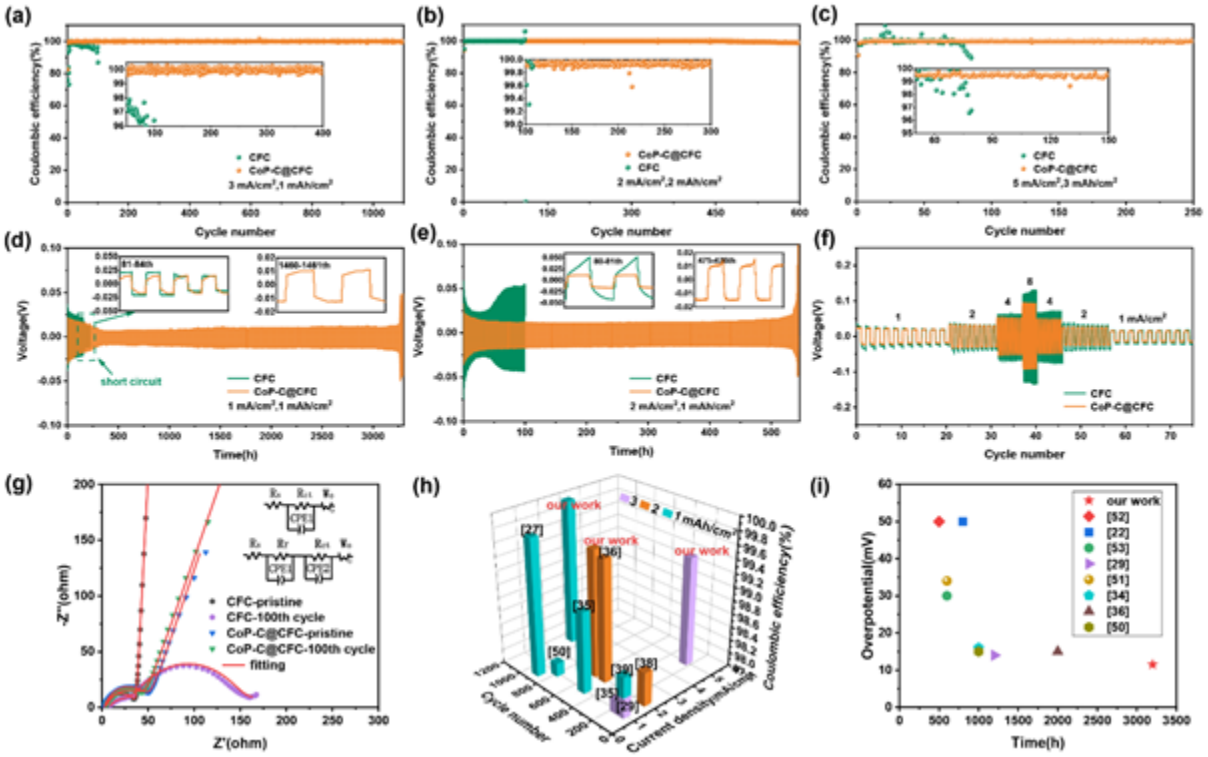

Fig. 6. Electrochemical performance of CoP-C@CFC electrodes. Coulombic efficiency of Li plating/striping on CFC and CoP-C@CFC electrode under different current density and area capacity (a-c). Cycling performance of symmetric cells with CFC-Li and CoP-C@CFC-Li anodes at different test

condition (d-e); (f) rate performance of symmetric cells with CFC-Li and CoP-C@CFC-Li anodes at various current densities from 1 to 8 mA cm^{-2} with a fixed deposition capacity of 1 mAh cm^{-2}. (g) Nyquist plots of CoP-C@CFC-Li anodes at different cycles with their corresponding charge transfer resistance. The performance comparison of half cells (h) and symmetric cells (i) between CoP-C@CFC and recently reported carbon fiber hosts.

capacity of 3 mAh cm^{-2} (Fig. S18g). Moreover, stable Li plating/stripping can be achieved, which is reflected in voltage-capacity curves (Fig. S18h). Notably, the folding processes of Li||CoP-C@CFC pouch cell with checking the LED illumination further demonstrate the structural stability of the 3D CoP-C@CFC host (Fig. S18a-f). When the CoP-C@CFC electrodes cycle over 50 cycles at 2 mA cm^{-2} with the total capacity of 2 mAh cm^{-2}, the surface of electrode is clean without Li dendrites and the CoP porous sheath still maintains undamaged (Fig. S19), while CFC electrodes show nonuniform Li distribution and much accumulated dead Li (Fig. S20). Comparatively, the half-cell performances of Co_3O_4-C@CFC at 3 mA cm^{-2} with a total capacity of 1 mAh cm^{-2} are shown in Fig. S21, which presents obvious shorter cycle lifespan originated from the formed insulative Li_2O_2 (Fig. S22).[24] Therefore, the high-performance of CoP-C@CFC is attributed to MOF-derived porous carbon sheath with embedded CoP nanoparticles, which uniforms Li^+/electron flux of carbon fiber surface and realizes optimized electrode kinetics.[25] Additionally, symmetric cells are assembled with CoP-C@CFC-Li prestored Li metal of 5 mAh cm^{-2}. As shown in Fig. 6d, CoP-C@CFC-Li anode exhibits stable voltage profile with a highly low overpotential of 11.5 mV and ultralong cycling life of 3200 h at 1 mA cm^{-2} with the capacity of 1 mAh cm^{-2} (20% DOD). However, sharply fluctuant voltage over 50 mV and short cycling lifespan less than 100 cycles have been displayed for CFC-Li anode. When the current density of 2 mA cm^{-2} is executed (Fig. 6e), the CoP-C@CFC anode can still maintain a stable cycling of about 550 h with a low voltage hysteresis of 13 mV, while the CFC-Li anode displays poor cycling and harsh overpotential. Additionally, excellent rate performance with low voltage polarizations of 15, 30, 50, 88 mV at 1, 2, 4 and 8 mA cm^{-2}, respectively, could be achieved in Fig. 6f. When the current density drops back to 4, 2, 1 mA cm^{-2}, the voltage polarization still keeps relatively stable values of 47, 26, 15 mV, respectively. It reveals that the CoP-C@CFC-Li anode exhibits excellent rate capability and high reversibility. By contrast, because of high nucleation barrier alongside with further exacerbated polarization, the CFC-Li anode displays a larger voltage hysteresis, especially under

realistic current density. The interfacial transfer impedance of Li^+ is studied by Electrochemical impedance spectroscopy (EIS) in half cells (Fig. 6g).[47,51] At pristine, the CoP-C@CFC-Li and CFC-Li electrodes show a low charge transfer resistance (R_{ct}) of 47.5 and 34.2 Ω, respectively. However, a low charge transfer resistance of 32.2 Ω can be maintained for CoP-C@CFC-Li anode after 100th cycles, while CFC-Li anode shows higher R_{ct} of 109.0 Ω. Meanwhile, the SEI layer of CoP-C@CFC indicates apparent peaks of Li_3P and LiF in high-resolution XPS profiles, while CFC shows strong peaks of Li_2O (Fig. S23). It reveals that superior conductivity and robust SEI layer are probably achieved in the CoP-C@CFC-Li electrodes, which owes to Li_3P@Co interface and stable 3D skeletons. Comparatively, charge transfer resistance continuously increases due to a mass of accumulated dead Li and weak SEI layer on the surface of CFC electrodes. Compared with the most recent reported carbon fiber-based Li host under similar testing conditions, CoP-C@CFC shows the best electrochemical performance with high CE and long cycling lifespan to our knowledge (Fig. 6h).[52] Meanwhile, symmetric cells at 20% DOD exhibit lowest overpotential and ultralong cycling time, while most infinite carbon fiber-based Li metal composite anodes have a large overpotential of over 20 mV after 500 h cycling under the same testing conditions (Fig. 6i).[53-55]

The potential application of CoP-C@CFC is further explored with full cell, which is assembled with CoP-C@CFC-Li anode and $LiFePO_4$ (LFP) cathode. As shown in Fig. 7a, CFC-Li||LFP full-cell exhibits a relatively high capacity at the initial stage, whereas the only reversible capacity of 76 mAh g^{-1} can be remained after 60 cycles at 1C. By comparison, CoP-

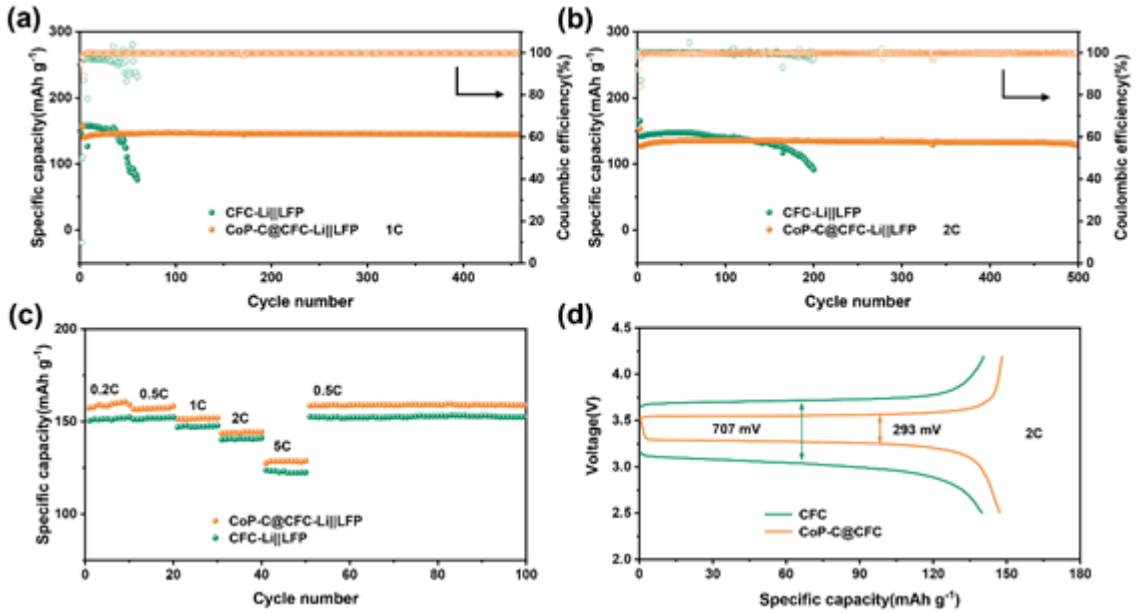

Fig. 7. Electrochemical performance of full cells. Cycling performance of CoP-C@CFC-Li||LFP at 1C (a) and 2C (b). Rate performance of CoP-C@CFC-Li||LFP (c). The charge/discharge profiles of CoP-C@CFC-Li||LFP at 2C (d).

C@CFC-Li||LFP full-cell possesses excellent cycling performance with discharge capacity of 145 mAh g^{-1} and the stable CE of 99.98% over 460 cycles, showing ultrahigh capacity retention of 98.6%. As the charge-discharge rate is enhanced to 2C (Fig. 7b), CoP-C@CFC-Li||LFP could hold discharge capacity of 130 mAh g^{-1} with a stable CE of 99.92% and a capacity retention of 95.8%. Comparatively, CFC-Li||LFP shows obvious poorer capacity retention ability with rapid decaying discharge capacity. To further demonstrate the applicability of the CoP-C@CFC, full cells with higher cathode loading of 5 mg cm^{-2} are provided, which still exhibit outstanding long cycling performance at 1C (Fig. S24a) and 2C (Fig. S24b). In addition, outstanding rate performance of CoP-C@CFC-Li||LFP has been achieved in coin cell (Fig. 7c). At low rate of 0.2C, a high reversible capacity of 161 mAh g^{-1} can be realized for CoP-C@CFC-Li anode, while CFC-Li anode merely maintains a discharge capacity of 151 mAh g^{-1}. With the rate increase to 5C, CoP-C@CFC-Li||LFP full cell always keeps reversible capacity of 129 mAh g^{-1}. When the rate is restored to 0.5C, a capacity of 160 mAh g^{-1} is attained again after 100 cycles without appreciable decay. However, CFC-Li||LFP full cell presents worse reversible capacity and poor rate performance under the same test conditions. Further, the charge/discharge profiles of the

two full cells have been exhibited in Fig. 7d. The voltage polarization of CoP-C@CFC-Li||LFP is 293 mV, which is obvious lower than CFC-Li||LFP (707 mV). In a word, these outstanding performances of full cells indicate MOF-derived porous carbon sheath with embedded CoP nanoparticles can enhance physicochemical property of CFC and obviously improve electrochemical cycling stability.

3. Conclusion

In summary, a 3D mix-conducting matrix decorated with MOF-derived porous carbon sheath with embedded CoP nanoparticles has been well-designed and fabricated by the scalable room-temperature crystallization and annealing-phosphating process. The CoP-C@CFC possesses excellent lithiophilicity and structural characteristics, which effectively increases specific surface area, highly reduces local current density and nucleation overpotential. In addition, the in-situ formed Li_3P@Co lithiophilic interface by the lithiation of CoP-C@CFC provides abundant Li nucleation sites and homogenizes Li-ion flux, which chronically suppress Li dendrites and volume effect. Thanks to these features, ultralong cycling lifespan of 1100 cycles with outstanding average Coulombic efficiency (CE) of 99.96% at practical current density of 3 mA cm^{-2} have been achieved. Under higher current density of 5 mA cm^{-2} with the realistic cycling capacity of 3 mAh cm^{-2}, CoP-C@CFC electrode also keeps superior average CE of 99.42% over 250 cycles. And the symmetric battery with finite CoP-C@CFC-Li anode exhibits a low overpotential of 11.5 mV over 3200 h at 1 mA cm^{-2} for 1 mAh cm^{-2} (20% DOD). When the full-cell is assembled with $LiFePO_4$ cathode and CoP-C@CFC-Li anode, it displays a capacity retention of 95.8% with 130 mAh g^{-1} over 500 cycles at 2C and shows excellent rate performance. Importantly, this work lights up MOF-derived metallic phosphide as 3D lithiophilic interface for flexible Li metal anodes.

Supporting Information

Supporting Information is available from the Wiley Online Library or from the author.

Acknowledgements

This work was supported by the National Natural Science Foundation of China (Grant No. 51874361, 52101278 and 52034011), the Science and Technology program of Hunan Province (2019RS3002 and 2020GK2074)

Conflict of Interest

The authors declare no conflict of interest.

Received: ((will be filled in by the editorial staff))
Revised: ((will be filled in by the editorial staff))
Published online: ((will be filled in by the editorial staff))

References

[1] F. Li, A. Thevenon, A. Rosas-Hernández, Z. Wang, Y. Li, C. M. Gabardo, A. Ozden, C. T. Dinh, J. Li, Y. Wang, J. P. Edwards, Y. Xu, C. McCallum, L. Tao, Z. Liang, M. Luo, X. Wang, H. Li, C. P. O Brien, C. Tan, D. Nam, R. Quintero-Bermudez, T. Zhuang, Y. C. Li, Z. Han, R. D. Britt, D. Sinton, T. Agapie, J. C. Peters, E. H. Sargent, *Nature* **2020**, *577*, 509.

[2] Y. Jiao, J. Qin, H. M. K. Sari, D. Li, X. Li, X. Sun, *Energy Storage Mater.* **2021**, *34*, 148.

[3] Y. Zhang, T. Zuo, J. Popovic, K. Lim, Y. Yin, J. Maier, Y. Guo, *Mater. Today* **2020**, *33*, 56.

[4] Y. Liu, Y. Elias, J. Meng, D. Aurbach, R. Zou, D. Xia, Q. Pang, *Joule* **2021**, *5*, 2323.

[5] D. Lin, Y. Liu, Y. Cui, *Nat. Nanotechnol.* **2017**, *12*, 194.

[6] H. Wang, J. He, J. Liu, S. Qi, M. Wu, J. Wen, Y. Chen, Y. Feng, J. Ma, *Adv. Funct. Mater.* **2021**, *31*, 2002578.

[7] W. Wahyudi, V. Ladelta, L. Tsetseris, M. M. Alsabban, X. Guo, E. Yengel, H. Faber, B. Adilbekova, A. Seitkhan, A. H. Emwas, M. N. Hedhili, L. J. Li, V. Tung, N. Hadjichristidis, T. D. Anthopoulos, J.

Ming, *Adv. Funct. Mater.* **2021**, *31*, 2101593.

[8] K. Wang, Q. Ren, Z. Gu, C. Duan, J. Wang, F. Zhu, Y. Fu, J. Hao, J. Zhu, L. He, C. Wang, Y. Lu, J. Ma, C. Ma, *Nat. Commun.* **2021**, *12*, 1.

[9] R. J. Y. Park, C. M. Eschler, C. D. Fincher, A. F. Badel, P. Guan, M. Pharr, B. W. Sheldon, W. C. Carter, V. Viswanathan, Y. Chiang, *Nat. Energy* **2021**, *6*, 314.

[10] Y. Zhu, J. Xie, A. Pei, B. Liu, Y. Wu, D. Lin, J. Li, H. Wang, H. Chen, J. Xu, A. Yang, C. Wu, H. Wang, W. Chen, Y. Cui, *Nat. Commun.* **2019**, *10*, 1.

[11] C. Niu, H. Lee, S. Chen, Q. Li, J. Du, W. Xu, J. Zhang, M. S. Whittingham, J. Xiao, J. Liu, *Nat. Energy* **2019**, *4*, 551.

[12] T. Mukra, E. Peled, *J. Electrochem. Soc.* **2020**, *167*, 100520.

[13] S. Zhou, I. Usman, Y. Wang, A. Pan, *Energy Storage Mater.* **2021**, *38*, 141.

[14] Z. Liang, K. Yan, G. Zhou, A. Pei, J. Zhao, Y. Sun, J. Xie, Y. Li, F. Shi, Y. Liu, D. Lin, K. Liu, H. Wang, H. Wang, Y. Lu, Y. Cui, M. P. C. U. SLAC National Accelerator Lab., *Sci. Adv.* **2019**, *5*, u5655.

[15] J. Pu, J. Li, K. Zhang, T. Zhang, C. Li, H. Ma, J. Zhu, P. V. Braun, J. Lu, H. Zhang, *Nat. Commun.* **2019**, *10*, 1.

[16] Y. Cheng, X. Ke, Y. Chen, X. Huang, Z. Shi, Z. Guo, *Nano Energy* **2019**, *63*, 103854.

[17] Y. Cheng, J. Chen, Y. Chen, X. Ke, J. Li, Y. Yang, Z. Shi, *Energy Storage Mater.* **2021**, *38*, 276.

[18] S. Fang, L. Shen, A. Hoefling, Y. Wang, G. Kim, P. A. van Aken, X. Zhang, S. Passerini, *Nano Energy* **2021**, *89*, 106421.

[19] H. Kwon, J. Lee, Y. Roh, J. Baek, D. J. Shin, J. K. Yoon, H. J. Ha, J. Y. Kim, H. Kim, *Nat. Commun.* **2021**, *12*, 1.

[20] H. Chen, Y. Yang, D. T. Boyle, Y. K. Jeong, R. Xu, L. S. de Vasconcelos, Z. Huang, H. Wang, H. Wang, W. Huang, H. Li, J. Wang, H. Gu, R. Matsumoto, K. Motohashi, Y. Nakayama, K. Zhao, Y.

Cui, *Nat. Energy* **2021**, *6*, 790.

[21] W. Ye, L. Wang, Y. Yin, X. Fan, Y. Cheng, H. Gao, H. Zhang, Q. Zhang, G. Luo, M. Wang, *ACS Energy Lett.* **2021**, *6*, 2145.

[22] S. Li, Q. Liu, J. Zhou, T. Pan, L. Gao, W. Zhang, L. Fan, Y. Lu, *Adv. Funct. Mater.* **2019**, *29*, 1808847.

[23] X. Yan, L. Lin, Q. Chen, Q. Xie, B. Qu, L. Wang, D. L. Peng, *Carbon Energy* **2021**, *3*, 303.

[24] C. Sun, A. Lin, W. Li, J. Jin, Y. Sun, J. Yang, Z. Wen, *Adv. Energy Mater.* **2019**, *10*, 1902989.

[25] Z. Luo, S. Li, L. Yang, Y. Tian, L. Xu, G. Zou, H. Hou, W. Wei, L. Chen, X. Ji, *Nano Energy* **2021**, *87*, 106212.

[26] B. Hong, H. Fan, X. Cheng, X. Yan, S. Hong, Q. Dong, C. Gao, Z. Zhang, Y. Lai, Q. Zhang, *Energy Storage Mater.* **2019**, *16*, 259.

[27] T. Yang, T. Qian, X. Shen, M. Wang, S. Liu, J. Zhong, C. Yan, F. Rosei, *J. Mater. Chem. A* **2019**, *7*, 14496.

[28] W. Zeng, X. Zhang, C. Yang, C. Zhang, H. Shi, J. Hu, Y. Zhao, W. Zhang, G. Zhang, H. Duan, *Chem. Eng. J.* **2021**, *412*, 128661.

[29] Y. Lu, J. Wang, Y. Chen, X. Zheng, H. Yao, S. Mathur, Z. Hong, *Adv. Funct. Mater.* **2021**, *31*, 2009605.

[30] S. Liu, X. Xia, Z. Yao, J. Wu, L. Zhang, S. Deng, C. Zhou, S. Shen, X. Wang, J. Tu, *Small Methods* **2018**, *2*, 1800035.

[31] S. Ye, F. Liu, R. Xu, Y. Yao, X. Zhou, Y. Feng, X. Cheng, Y. Yu, *Small* **2019**, *15*, 1903725.

[32] Y. Mei, J. Zhou, Y. Hao, X. Hu, J. Lin, Y. Huang, L. Li, C. Feng, F. Wu, R. Chen, *Adv. Funct. Mater.*, https://doi.org/10.1002/adfm.202106676.

[33] H. Shen, F. Qi, H. Li, P. Tang, X. Gao, S. Yang, Z. Hu, Z. Li, J. Tan, S. Bai, F. Li, *Adv. Funct. Mater.* **2021**, *31*, 2103309.

[34] J. Zhu, J. Chen, Y. Luo, S. Sun, L. Qin, H. Xu, P. Zhang, W. Zhang, W. Tian, Z. Sun, *Energy Storage Mater.* **2019**, *23*, 539.

[35] M. Zhu, J. Zhang, Y. Ma, Y. Nan, S. Li, *Carbon* **2020**, *168*, 633.

[36] Y. Fang, W. Cai, S. Zhu, K. Xu, M. Zhu, G. Xiao, Y. Zhu, *J. Energy Chem.* **2021**, *54*, 105.

[37] T. S. Wang, X. Liu, Y. Wang, L. Z. Fan, *Adv. Funct. Mater.* **2021**, *31*, 2001973.

[38] T. Zhou, J. Shen, Z. Wang, J. Liu, R. Hu, L. Ouyang, Y. Feng, H. Liu, Y. Yu, M. Zhu, *Adv. Funct. Mater.* **2020**, *30*, 1909159.

[39] G. Jiang, N. Jiang, N. Zheng, X. Chen, J. Mao, G. Ding, Y. Li, F. Sun, Y. Li, *Energy Storage Mater.* **2019**, *23*, 181.

[40] L. Chen, G. Chen, W. Tang, H. Wang, F. Chen, X. Liu, R. Ma, *Mater. Today Energy* **2020**, *18*, 100520.

[41] D. Liang, H. Jiang, Q. Xu, J. Luo, Y. Hu, C. Li, *J. Electrochem. Soc.* **2018**, *165*, F1286.

[42] Z. Wang, J. Shen, J. Liu, X. Xu, Z. Liu, R. Hu, L. Yang, Y. Feng, J. Liu, Z. Shi, L. Ouyang, Y. Yu, M. Zhu, *Adv. mater.* **2019**, *31*, e1902228.

[43] H. Su, Y. Zhang, X. Liu, F. Fu, J. Ma, K. Li, W. Zhang, J. Zhang, D. Li, *J. Colloid Interf. Sci.* **2021**, *582*, 969.

[44] D. Liu, W. Lu, K. Wang, G. Du, A. M. Asiri, Q. Lu, X. Sun, *Nanotechnology* **2016**, *27*, 42.

[45] H. Jiang, H. Fan, Z. Han, B. Hong, F. Wu, K. Zhang, Z. Zhang, J. Fang, Y. Lai, *J. Energy Chem.* **2021**, *54*, 301.

[46] N. Wu, Y. Li, A. Dolocan, W. Li, H. Xu, B. Xu, N. S. Grundish, Z. Cui, H. Jin, J. B. Goodenough, *Adv. Funct. Mater.* **2020**, *30*, 2000831.

[47] H. Jiang, Y. Zhou, H. Zhu, F. Qin, Z. Han, M. Bai, J. Yang, J. Li, B. Hong, Y. Lai, *Chem. Eng. J.* **2022**, *428*, 132648.

[48] Z. Liu, S. Yang, B. Sun, X. Chang, J. Zheng, X. Li, *Angew. Chem. Int. Ed. Engl.* **2018**, *57*, 10187.

[49] K. Guo, B. Xi, R. Wei, H. Li, J. Feng, S. Xiong, *Adv. Energy Mater.* **2020**, *10*, 1902913.

[50] L. Gao, J. Li, B. Sarmad, B. Cheng, W. Kang, N. Deng, *Nanoscale* **2020**, *12*, 14279.

[51] J. Wang, W. Huang, A. Pei, Y. Li, F. Shi, X. Yu, Y. Cui, *Nat. Energy* **2019**, *4*, 664.

[52] Y. Fang, S. L. Zhang, Z. Wu, D. Luan, X. W. D. Lou, *Sci. Adv.* **2021**, *7*, g3626.

[53] P. Zhang, C. Peng, X. Liu, F. Dong, H. Xu, J. Yang, S. Zheng, *ACS Appl. Mater. Inter.* **2019**, *11*, 44325.

[54] B. Liu, Y. Zhang, G. Pan, C. Ai, S. Deng, S. Liu, Q. Liu, X. Wang, X. Xia, J. Tu, *J. Mater. Chem. A* **2019**, *7*, 21794.

[55] L. Tao, A. Hu, Z. Yang, Z. Xu, C. E. Wall, A. R. Esker, Z. Zheng, F. Lin, *Adv. Funct. Mater.* **2020**, *30*, 2000585.

An ion/electron redistributed 3D flexible host is designed by lithiophilic carbon fiber cloth modified with MOF-derived porous carbon sheath with embedded CoP nanoparticles (CoP-C@CFC). During the Li plating, the in-situ formed Li_3P@Co conductive interface on CoP-C@CFC realizes Li^+/charge redistribution, which achieves highly average Coulombic efficiency of 99.96% over 1100 cycles at practical current density of 3 mA cm^{-2}.

Huai Jiang, Yangen Zhou, Caohong Guan, Maohui Bai, Furong Qin, Maoyi Yi, Jie Li, Bo Hong, Yanqing Lai**

Ion/electron redistributed 3D flexible host for achieving highly reversible Li metal batteries